IEEE Access
Multidisciplinary | Rapid Review | Open Access Journal

Date of publication xxxx 00, 0000, date of current version xxxx 00, 0000.

Digital Object Identifier 10.1109/ACCESS.2017.Doi Number

Coverage Extension of Indoor 5G Network using RoF-based Distributed Antenna System

Eon-Sang Kim[1], Minkyu Sung[1], Jong Hyun Lee[1], Joon Ki Lee[1], Seung-Hyun Cho[1], and Joonyoung Kim[2]

[1]Optical Network Research Section, Electronics and Telecommunications Research Institute, 218 Gajeong-ro, Yuseong-gu, Daejeon, 34129 Korea
[2]Dept. of Smart Information and Communications Engineering, Sangmyung University, 31 Sangmyungdae-gil, Dongnam-gu, Cheonan-si, 31066 Korea

Corresponding author: Joonyoung Kim (e-mail: joonyoung.kim@smu.ac.kr).

This work was partially supported by Electronics and Telecommunications Research Institute (ETRI) grant funded by the Korean government [20ZH1100, Study on 3D communication technology for hyper-connectivity] and was also partially supported by 'The Cross-Ministry Giga KOREA Project' grant funded by the Korea government Ministry of Science, ICT and Future Planning (MSIT) (No. GK19N0300, Development of Indoor DAS Technology based on IFoF for 5G Mobile Communication).

ABSTRACT We propose and demonstrate a cascaded distributed antenna system (DAS) for efficiently extending the coverage of the mmWave-based 5G indoor network. For this, we exploit the radio-over-fiber (RoF) system based on the intermediate-frequency-over-fiber (IFoF) transmission technique that is enabled to add/drop the specific wavelength to the designated remote antenna unit (RAU) with using optical splitters and coarse wavelength division multiplexing (CWDM) filters. Moreover, the IFoF transceivers (TRx) perform the subcarrier multiplexing (SCM) in order to transmit 2×8 frequency allocation (FA) 5G signals per a single optical carrier, where each FA has 100 MHz bandwidth, leading each RAU to support 2×2 MIMO operation. Consequently, the cascaded structure allows for the adaptive and flexible configuration of the order of MIMO in accordance of the required data throughput at the specific indoor area. We introduce the cascaded IFoF link structure that can support up-to 13.5 dB optical power budget with following error-vector-magnitude (EVM) performance characterizations. And then we experimentally demonstrate the RoF-based cascaded DAS network, showing that more than 1 Gb/s total throughput can be achieved per a single antenna. Furthermore, we examine the use of avalanche photodiode (APD) to further increase the optical power budget (i.e., the coverage) based on experiment as well as simulation.

INDEX TERMS 5G communication system, cascade, distributed antenna system, millimeter wave, radio-over-fiber

I. INTRODUCTION

In mobile telecommunications, the millimeter wave (abbreviated mmWave) is drawing increasing attention as it provides abundant spectrum to enable the emergence of diverse next-generation applications. As such, the 5G network is evolving from the mid-bands (i.e., 1-6 GHz) to the mmWave (i.e. 24-60 GHz)-based services that will be delivering multi-gigabit speeds to end-users, consequently allowing for the realization of the ultimate 5G scenarios such as enhanced mobile broadband (eMBB) as well as ultra-reliable and low-latency communications (URLLC) and massive internet of things (mIoT) [1], [2]. However, the deployment of such high frequency-based mobile network introduces new technical challenges compared to the low- and mid-band services. Firstly, the mmWaves propagate shorter distance (i.e., experiences larger line-of-sight (LOS) path loss) than that of sub-6GHz waves, leading to the smaller cell size and/or higher-powered radio stations [3]. In addition, the mmWaves do not propagate through many of the external/internal building materials such as concrete walls and tinted windows [4], [5]. Another challenge concerns the poor diffraction characteristics or high directivity, as the "light" does, resulting in the shadow areas where the network speed significantly drops [4], [5]. Thus, it is extremely important to secure the proper technical tools to bring the mmWave 5G service indoors where over 80 % of mobile data is being consumed [6], [7].

The small cell in support of advanced MIMO technology may be considered for deploying and extending the 5G indoor network. In spite of its advantages such as low unit

This article has been accepted for publication in a future issue of this journal, but has not been fully edited. Content may change prior to final publication. Citation information: DOI 10.1109/ACCESS.2020.3033592, IEEE Access

cost and simple installations, the small cell is not appropriate solution to support multiple providers in the large-scale venues [6], [7]. Moreover, it does not flexibly support the scaling and reconfiguration of the network. A notable alternative to the small cell is a distributed antenna system (DAS) that was primarily used to extend the indoor network coverage in the previous mobile eras (i.e. 2G, 3G, and LTE). The DAS comprises a centralized main hub unit (MHU), e.g., on the roof of buildings and multiple remote antenna units (RAU) spatially distributed throughout the indoor area, where the RF/fiber-optic cabling is employed between the MHU and RAUs [7]. Consequently, the DAS network allows to literally distribute the signal across many low-power antenna points inside the building.

Evolving from 2G to LTE, the simple RF cabling of the passive DAS was replaced by the digital fiber-optic transmission technology, leading to the emergence of active DAS. The active DAS captures and digitizes the mobile signal based in the standard protocols such as Common Public Radio Interface (CPRI) [8], [9]. Although this solution solved many RF cabling-induced problems of the passive DAS network, it was at the expense of the system cost and complexity. Additionally, the digitization step makes the network reconfiguration challenging and inflexible as the small cells do. More importantly, the broadband 5G signal leads the fiber-optic link to handle hundreds of Gb/s transmission, which would be highly costly [9].

One of merits of the fiber-optic link is its great dynamic range (e.g., >100 dB·Hz$^{2/3}$) as well as the broad bandwidth (e.g., a tens of GHz) [10]. It indicates that one does not necessarily need to include the digitization step for the DAS network where the transmission distance would be normally less than a few km. Instead, one may seamlessly transport the radio (e.g., 64-QAM OFDM 5G) signal throughout the fiber-optic network without making use of the analog-to-digital (A/D) and digital-to-analog (D/A) converters, which is called the Radio-over-Fiber (RoF) transmission [11]. Thus, the RoF technology makes the active DAS more flexible and efficient as the passive DAS used to be, which is to be an eminent solution for delivering the mmWave-based 5G services to indoor users in large-scale indoor facilities such as university, stadium, corporate buildings, and so on.

The RoF is categorized into: i) Radio Frequency-over-Fiber (RFoF) and ii) Intermediate Frequency-over-Fiber (IFoF). In the RFoF, the mobile signal at mmWave-band is optically transported using high-speed (e.g. a tens of GHz) photonic devices (e.g. electro-optic modulators and wideband photodiodes) that increase the system cost [12]. Moreover, the dispersion-induced RF power fading degrades the quality of signal at mmWave bands [13]. Another option for realizing the RFoF is to utilize the optical heterodyning of two different optical sources [14]. However, it requires extra circuitries to stabilize the frequency and phase of the generated mmWave signal (at RAU) to the reference clock in the MHU. Although the optical frequency comb could be alternatively employed to generate the frequency-stabilized mmWave at RAU, its phase is still unlocked, and more importantly, it increases the system complexity, making it difficult to manage the system on a long-term basis [15]. In the IFoF, on the other hand, the mobile signal is down-converted to IF-band (e.g., 2 GHz) prior to the fiber-optic transmission. Thus, it prevents the 5G signal from the dispersion-induced quality degradation with no use of extra optical devices such as reference lasers and optical frequency comb. In addition, the IFoF link can be implemented using relatively low speed devices (e.g. directly modulated laser diode and relatively low-speed photodiodes that are less costly), while the RAU is supposed to include the IF-to-mmWave conversion module. We proposed and demonstrated the IFoF-based DAS network for providing the mmWave-based 5G services to indoors as well as outdoors, achieving up-to ~9 Gb/s end-user throughput [16], [17]. However, it was based on the simple point-to-point configuration that did not demonstrate the full potential of the RoF-based DAS network in terms of the coverage extension, management, flexibility, and so on.

In this paper, we introduce the cascaded DAS architecture using the RoF transmission technology. The cascade structure allows for the enhanced scaling and reconfiguration characteristics, effectively eliminating the shadow areas that are simulated based on the 3D ray tracing in the following section. Especially, the coverage as well as capacity can be easily extended as required through installing additional RAUs at the hotspot area. In addition, it will ease the installation and management of the system and the infrastructure (e.g., fiber-optic cables), subsequently reducing the related expenditures as well. In the following sections, we discuss the detailed configurations and transmission performances of the cascaded RoF system. We also perform the throughput measurement for the various single mode fiber (SMF) lengths and the wireless distances. Additionally, we investigate the use of avalanche photodiode (APD) in the RoF link for further extension of the coverage based on simulation in conjunction with the actual experiment.

II. CASCADED DISTRIBUTED ANTENNA SYSTEM

The signal is largely attenuated as the mmWave-band signal is propagating across the exterior wall of building, which is called the outdoor-to-indoor (O2I) penetration loss. The 3GPP technical report specifies the O2I penetration loss for different kind of building materials in [3]. For example, the outer wall made of concrete typically induces attenuation of 5+4f dB, where f represents the frequency in GHz. Thus, the power of the mmWave signal, e.g., at 28 GHz band is expected to decrease by 117 dB due to the O2I penetration loss. In addition, the unique indoor environments, comprising a lot of walls, doors, windows, staircases, ceilings, etc. made of many different kinds of building materials, would lead to additional signal attenuations as reported in [4]. For example, the typical attenuations by tinted glasses and internal walls would be 24.5 dB/cm and 7 dB/each, respectively. [4].

This article has been accepted for publication in a future issue of this journal, but has not been fully edited. Content may change prior to final publication. Citation information: DOI 10.1109/ACCESS.2020.3033592, IEEE Access

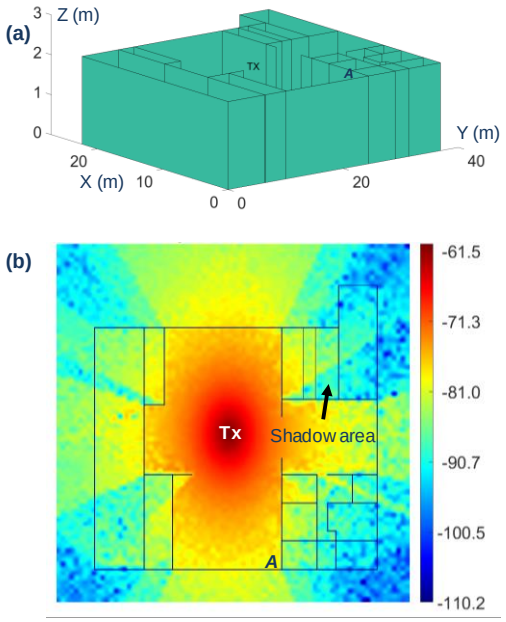

FIGURE 1. **(a) Indoor layout for the 3D ray-tracing simulation and (b) the simulated received signal power in dBm where the transmitter (Tx) is a mmWave (i.e., 28 GHz) dipole antenna that is at the height of 2.2 meters.**

More importantly, the mmWaves have much higher LOS path loss (PL_{LOS}) than that of sub-6GHz signal, where the LOS path loss is proportional to a square of the carrier frequency and the wireless distance. Based on the experimental surveys, the LOS path loss was characterized to be [3]:

$$PL_{LOS} = 32.4 + 17.3\log_{10}(d) + 20\log_{10}(f_c) \qquad (1)$$

where d is the wireless distance in meter (e.g., typically 1-150 meters for indoors) between the transmitter (Tx) and receiver (Rx), and f_c is the carrier frequency in GHz. Thus, the LOS path loss at 28 GHz will be 73.4 dB after 5 m wireless transmission. Furthermore, the complex internal structure of buildings will result in multiple reflections as well as refractions, resulting in waveguiding effects [4]. Even though one utilizes the building materials featuring small losses to the mmWaves, the waveguiding effects could give rise to the shadow areas.

Thus, we investigate the impacts of LOS path loss, refractions, and multiple reflections on the network coverage by performing the 3D ray-tracing simulation based on the Fermat's principle of least time, which is to define the ray path travelling from the source to destination in a given condition [18]. Specifically, we used the image method to take multiple reflections (up-to 2nd reflection in our simulation) into consideration. The indoor layout is illustrated in Fig. 1a. We supposed the use of concrete walls that have the relative permittivity of 5.31 as described in [3]. We also assumed that the walls have zero thickness in order to neglect effects of the penetration loss. The ceiling height was set to be 2.2 meters where the Tx is supposed to be installed on the ceiling as shown in Fig. 1a. The Tx was a dipole antenna where the total output power is +20 dBm with vertical polarization.

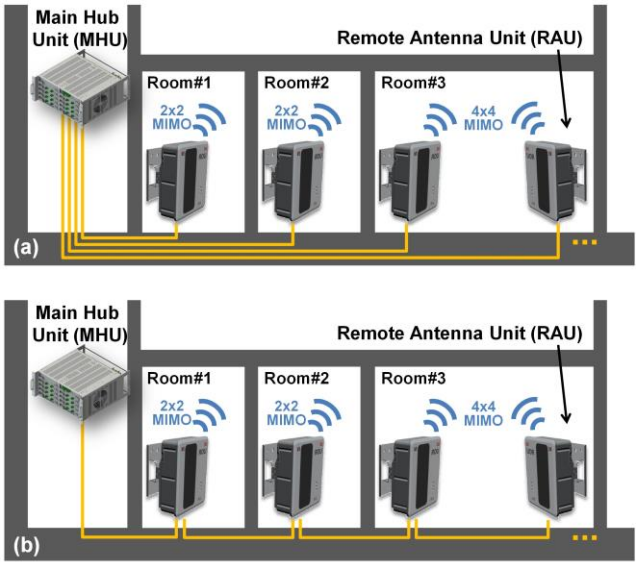

FIGURE 2. **Distributed antenna system (DAS) based on (a) conventional point-to-point structure and (b) cascade structure that provides better scalability.**

The result of ray-tracing simulation, illustrated in Fig. 1b, shows the power level of the received mmWave signal represented in dBm at 1 m height at which the Rx is located. At the position-*A* (in Fig. 1) where the Rx is ~10 meters away from the Tx, the received power decreases to below -80 dBm even though there is no blockage on the signal path. The received power at *A* is lower by ~20 dB when compared to that nearby the Tx, which is in line with Eq. 1. The oscillating characteristics (seen as the "dots" in Fig. 1b) are due to the interference between the signal and the reflected waves. More importantly, we observe the shadow areas behind the walls due to the refractions, especially in case the ray's incident angle to the wall is close to 90°. The network coverage will be much more reduced than the observation in Fig. 1b, once we take the penetration loss into account, as already discussed.

The DAS relieves the coverage issues in the mmWave-based indoor 5G network as Fig. 2 illustrates. In reality, the most common architecture of the DAS would be the point-to-point system where the optical transceiver (TRx) cards in MHU are connected to RAUs one by one, as depicted in Fig. 2a. This guarantees the quality of service (QoS) and reliability at the expense of cost and flexibility. An alternative would be the cascade structure that is illustrated in Fig. 2b. In this method, as its name implies, multiple RAUs are connected in series to a single TRx card of the MHU using optical power splitters and CWDM filters. This enables efficient scaling and reconfiguration, and requires less fiber-optic infrastructures, making the system highly practical. Another merit of this cascade structure is that the multi-RAUs share the fiber-optic cable to transmit the uplink signals. This suppresses the thermal- and mechanical-perturbation-induced phase drift between the uplink channels, subsequently reducing the burdens of phase noise/offset compensation at the 5G base-station [19].

This article has been accepted for publication in a future issue of this journal, but has not been fully edited. Content may change prior to final publication. Citation information: DOI 10.1109/ACCESS.2020.3033592, IEEE Access

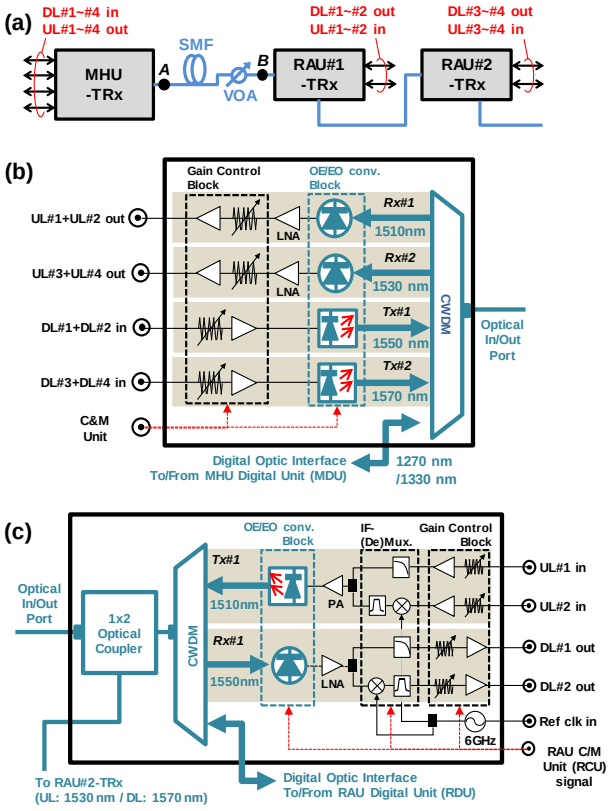

FIGURE 3. (a) Cascaded intermediate frequency over fiber (IFoF) link, and schematic diagrams of (b) the main hub unit-transceiver (MHU-TRx) and (c) the remote antenna unit#1-transceiver (RAU#1-TRx).

However, the cascaded optical power splitters on the fiber-optic link will significantly decrease the received optical power, which may result in the QoS degradation. Thus, in the following section, we introduce the cascade-structured RoF system, and characterize the error-vector-magnitude (EVM) and throughput performances.

III. EXPERIMENTAL SETUP AND RESULTS

Fig. 3a shows the IFoF system to realize the cascaded DAS network. The fiber-optic link delivers the 5G signals at the IF bands in two directions: i) downlink (DL: from MHU-Tx to RAU-Rx) and uplink (UL: from RAU-Tx to MHU-Rx). We used two RAUs in the experiment, though we inserted the variable optical attenuator (VOA) that gives additional optical loss of 6.5 dB, corresponding to two of 1×2 optical splitters (or a single 1×4 optical splitter). Thus, the total optical attenuation was ~10.2 dB for the MHU-RAU#1 link (i.e., three 1×2 optical splitters) and ~13.5 dB for the MHU-RAU#2 link (i.e., four 1×2 optical splitters) with 2 km SMF's loss (0.5 dB at 1550nm) included as well. Note that the last RAU of the IFoF link (which would be following RAU#2 in Fig. 3a) would not contain the optical splitter.

The schematic diagrams of TRx are shown in Fig. 3b and 3c. The MHU-TRx (Fig. 3b) comprises a gain control block and an OE/EO conversion block. The gain control block consists of RF amplifiers and attenuators in order to adjust the electrical power of the IF-signal. The OE/EO conversion

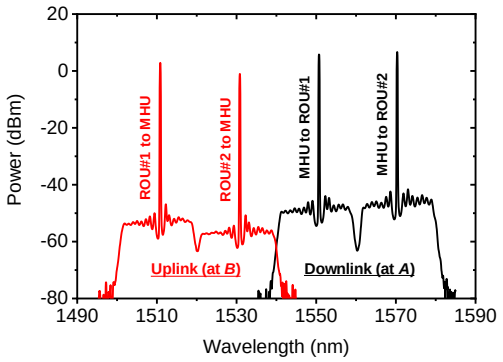

FIGURE 4. Measured optical spectrum of uplink (1510 and 1530 nm) and downlink (1550 and 1570 nm) signals at the intermediate frequency over fiber (IFoF) link.

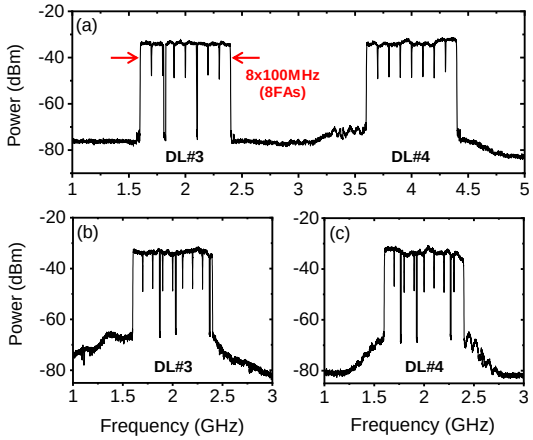

FIGURE 5. Electrical spectrum of (a) input signal of MHU-TRx (DL#3+DL#4), (b) output signal of DL#3, and (c) output signal of DL#4 transferred by 1570 nm optical carrier (DL: downlink).

block includes the PIN-PD and the distributed feedback laser diode (DFB-LD), which are not thermal-stabilized, i.e., uncooled. Instead, we actively controlled the bias current of the LDs using the integrated monitoring PD to keep the constant output power (+6 dBm each). The RAU-TRx (see Fig. 3c) has three blocks: the gain control block, OE/EO conversion block, and IF-Mux block. The IF-Mux block performs the subcarrier (de-)multiplexing (SCM) of two IF-band signals in order to double the transmission capacity per wavelength [12]. For this, we utilized the RF-mixers driven by 6 GHz local oscillator (LO) signal that is produced by the phase locked loop (PLL)-integrated voltage-controlled oscillator (VCO). The MHU has the IF-Mux module for SCM outside the TRx card as will be explained in the throughput measurement setup. Note that Fig. 3c shows the RAU#1-TRx where the RAU#2-TRx is identical to RAU#1-TRx except the wavelengths.

In the experiment, we used four wavelengths: 1510 and 1530 nm for uplinks, and 1550 and 1570 nm for downlinks (see Fig. 4) which were selected amongst the CWDM 18 channels that have 20 nm guard band that is wide enough to avoid optical beating noise of uncooled DFB-LDs. Moreover, each channel in TRx is spatially isolated from

This article has been accepted for publication in a future issue of this journal, but has not been fully edited. Content may change prior to final publication. Citation information: DOI 10.1109/ACCESS.2020.3033592, IEEE Access

others using metal enclosures we designed and produced to prevent inter-channel electromagnetic interference (EMI).

In the DL, the 1550 nm and 1570 nm signals are dropped into the RAU#1-Rx and RAU#2-Rx, respectively, through the optical couplers and CWDMs. In the UL, on the other hand, the 1530 nm signal of RAU#2-Tx is combined to the 1510 nm signal by the optical coupler of the RAU#1-TRx. If a larger number of RAUs (than 2) are in use, one may need to employ more wavelengths.

Based on the SCM realized by the IF-Mux blocks, each optical carrier transfers 2×8 frequency allocations (FAs), each FA has 100 MHz-bandwidth 64-QAM OFDM signal with subcarrier spacing of 120 kHz, as shown in Fig. 5. In the DL, the MHU's IF-Mux module performs the SCM, delivering 2×8FA signals (at 1.6-2.4 GHz and 3.6-4.4 GHz) to the DFB-LD of MHU-Tx. For example, Fig. 5a shows the spectrum of combined DL#3 and DL#4 signal measured at the input port of the MHU-Tx#2 (at 1570 nm) that is to be transmitted towards the RAU#2-Rx. At the end of the RAU#2-Rx, the SCM signal is de-multiplexed by the IF-Mux block into DL#3 and #4, respectively, as shown in Fig. 5b and 5c. Fig. 5 shows that the spectral shape of the 5G signal is well preserved after the IFoF transmission. The FA-dependent link gain varied by less than ±1.5 dB within the signal bandwidth that was achieved by optimized impedance matching of the OE/EO conversion parts and electrical signal paths. In the UL transmission, two IF-signals (at 1.6-2.4 GHz band) are multiplexed by the IF-Mux block of the RAU-Tx to be transmitted to the MHU-Rx.

The input RF power of the 2×8FA signals (i.e. DL#3 and #4) was -7 dBm. We set the RF gain of the RoF-link by means of the gain control blocks in Rxs to be 0 dB, maintaining -7 dBm output power of the Rxs during the operation. In addition, we utilized the gain control blocks in Txs to implement the IFoF transmission system at the optimum optical modulation index (OMI) [16], [20].

In the complete RoF setup, the RAUs include the module for the frequency conversion between the IF-band (1.6-2.4 GHz) and the mmWave-band (28 GHz). We experimentally confirmed that the mmWave conversion unit (abbreviated mmU)-induced EVM degradation was less than 3 % when the phase noise of the 10 MHz reference clock is lower than -120 dBc/Hz at 10 kHz offset [16]. Since 3GPP suggests the EVM level of the 64QAM signal to be 8 % or less at the antenna site, we consider the IFoF link is supposed to have the EVM level less than 5 %.

The EVM performance of the IFoF link is mainly determined by two factors: i) the noise (thermal noise, shot noise, and relative intensity noise) and ii) the nonlinear distortions, particularly by nonlinear responses (including signal clipping) of RF amplifiers and optoelectronic devices such as LDs and PDs. As aforementioned, we utilized the gain control blocks in Txs to operate the IFoF system at the optimum point where the net effects of the noise and the nonlinear distortion becomes minimum [16], [20]. At the low received optical power (e.g., -5 dBm for RAU#1 and -8 dBm

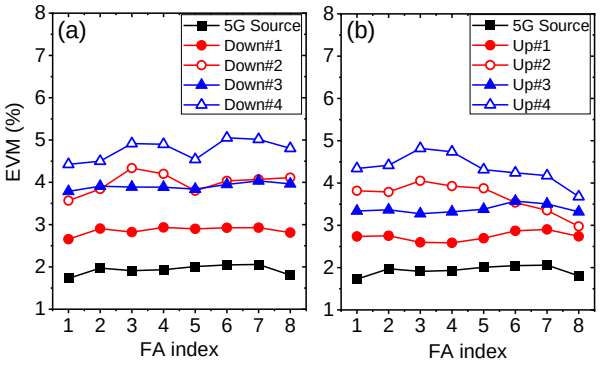

FIGURE 6. Measured error vector magnitude (EVM) values of the cascaded intermediate-frequency-over-fiber (IFoF)-link: (a) downlink#1~#4 and (b) uplink#1~#4.

for RAU#4 in our case), however, the thermal/shot noise become the dominant limiting factors. To be more specific, the relative noise floor was about -27 dB while the nonlinear distortion term, including the 3rd order intermodulation distortions (IMD3), was less than -33 dB compared to the signal power.

Other than those two factors (noise and nonlinear distortion), the chromatic dispersion (CD) of the used standard SMF (G.652.D in our system) may induce additional performance degradation. To be more specific, the CD interacts with the positive chirp of the directly modulated laser, producing the 2nd order IMD (IMD2) [16] [21]. This affects even number channels (i.e., 3.6-4.4 GHz) at which the IMD2 components of the odd number channel (i.e., 1.6-2.4 GHz) signals are located, though it was not significantly observed in our 2 km link. Moreover, the CD results in the multi-path propagation effects in the fiber-optic link, which is estimated to be <3 ps after 2 km transmission in C-band, being negligible as compared to the cyclic prefix duration.

Fig. 6 shows the measured EVM values after (a) DL and (b) UL transmission of the IFoF system. Even number channels (#2 and #4) show relatively larger EVM values than that of odd number channels (#1 and #3), which is attributed to the excess noise by the IF-Mux unit that includes the RF-mixers and passive components such as RF filters and splitters. On the other hand, RAU#2 (see #3 and #4) shows rather worse performance than RAU#1 (see #1 and #2) as the RAU#2 experiences more optical attenuation (of ~3.3 dB) due to the 1×2 optical splitter in the TRx. All channels (#1~#4), however, met the EVM requirement (5 %). This means that the IFoF system could effectively accommodate the cascaded architecture should its total optical link loss is less than 13.5 dB. The uneven EVM level (according to the RAUs) could be improved by utilizing alternative optical power splitting ratios (e.g. utilizing 90:10 instead of 50:50).

We characterized the throughput performance of the cascaded DAS system using the complete RoF link setup illustrated in Fig. 7. We used four channels of Korea Telecom (KT) 5G base station, delivering 4×8 FAs signals to the input (DL#1~DL#4) of the MHU which is a rack-

This article has been accepted for publication in a future issue of this journal, but has not been fully edited. Content may change prior to final publication. Citation information: DOI 10.1109/ACCESS.2020.3033592, IEEE Access

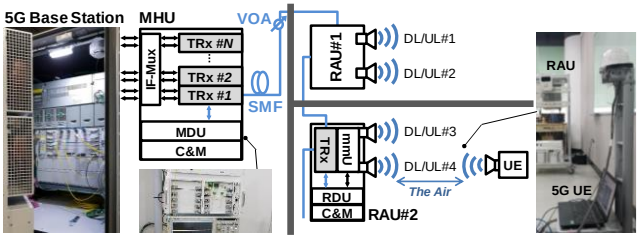

FIGURE 7. Experimental setup for the throughput measurement of the cascaded radio-over-fiber (RoF)-based distributed antenna system (MDU: MHU Digital Unit, RDU: RAU Digital Unit, C&M: Control and Management, mmU: mmWave conversion Unit, UE: User Equipment).

mounted module that can contain up to 8 TRx cards (one TRx-card used only in this experiment). Then the IF-Mux units of MHU perform the SCM, multiplexing two IF-band signals as already explained in Fig. 5a. Note that we enabled the dynamic modulation and coding scheme (MCS) during the throughput measurement by which the modulation format was automatically optimized according to the channel condition. However, we restricted the upper limit of MCS to 64-QAM in order to remain consistent with the EVM characterization, and also to perform reliable measurement.

The SMF length was limited up to 300 m. For the SMF longer than 300 m, the 5G base station lost its connection to the RAUs, which could be resolved with enabling the timing advance (TA) technique. The MHU is in support of the TA function, providing the 5G base station with the RAU's response time upon the request from MHU (which could be used to obtain the actual distance). The TA function can compensate the delay of up-to 100 μs that corresponds to the roundtrip time of 10 km long SMF. However, for the SMF longer than 2 km, the EVM level would be degraded due to the CD of the SMF. Thus, to extend the fiber length to the TA limit, the RoF link is required to use O-band where the CD-induced penalty is minimized. The actual total length of the SMF used in the experiment was about 330 m including the fiber-optic cable between the MHU and RAUs.

The output DL signal of the RAU-TRx (at IF-band) is delivered to the mmU for up-conversion from the IF-band to the mmWave band (27.5~28.3 GHz), where the frequency error was measured to be less than ±0.0003 ppm (part-per-million). The total output power of the mmWave signal at the RAU was +20 dBm per antenna. In case of the UL, the mmU of the RAU down-converts the mmWave mobile signal to the IF-band for the IFoF transmission.

The RoF link has an auxiliary channel based on the digital optic transmission that is realized by the MHU digital unit (MDU) and RAU digital unit (RDU). In the digital optic link, we used 1270 nm for DL and 1330 nm for UL which are wavelength-division multiplexed with the 5G signals (i.e., at 1510, 1530, 1550, 1570 nm) using the CWDM filter. The auxiliary link offers three different functions: i) time division duplexing (TDD)-signal transfer, ii) 10 MHz clock distribution to RAUs, and iii) the system control and management (C&M). The 5G DAS network operates based

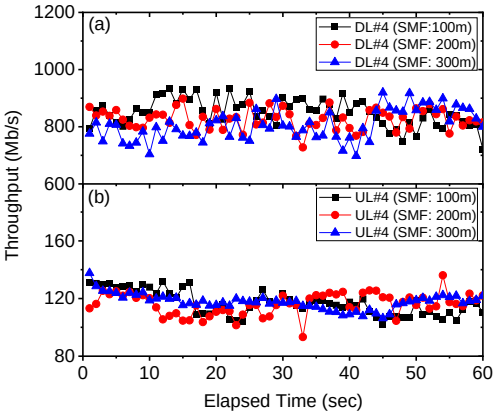

FIGURE 8. Measured throughput for the various SMF lengths at (a) the downlink#4 (DL#4) and (b) of the uplink#4 (UL#4). We presume channels #1~#3 have the throughput performances that are equal to or better than channel #4.

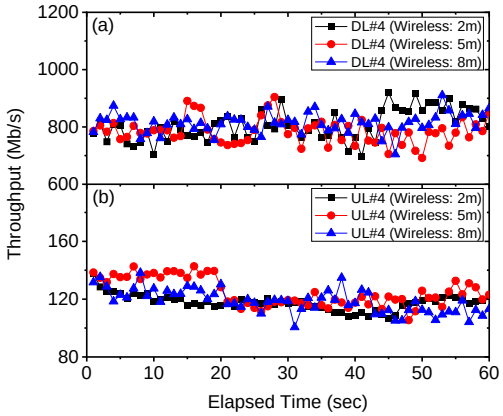

FIGURE 9. Measured throughput for the various air distances of (a) the downlink#4 (DL#4) and (b) of the uplink#4 (UL#4). We presume channels #1~#3 have the throughput performances that are equal to or better than channel #4.

on TDD, where the ratio of DL and UL was 8:1, respectively, preventing the interference between the DL and UL. For this, we transfer the TDD signal to the RAUs' mmU that include the RF switches driven by the transferred TDD signal. Also, the mmU has an oscillator that is frequency-/phase-locked to the reference clock source. Thus, the digital optic link delivers the 10 MHz clock signal from MHU to RAUs which is also used for PLL of the TRxs' IF-Mux blocks.

We used RAU#2 to measure the throughput that was placed in a different room from the MHU. We show the throughput results of DL#4/UL#4 which has the worst EVM performances, as seen in Fig. 6. The UE is equipped with Giga-bit Ethernet network adaptor based on SISO-operation, thus we characterized each antenna port independently [16]. As aforementioned, however, each RAU comprises a pair of antenna based on polarization multiplexing to support 2×2 MIMO service. Furthermore, the MIMO could be scaled up to 4×4 through the simultaneous use of two RAUs (with adequate distance between those). Then, the RoF link will deliver 4-channel signals (4 × 800 MHz) that are post-

This article has been accepted for publication in a future issue of this journal, but has not been fully edited. Content may change prior to final publication. Citation information: DOI 10.1109/ACCESS.2020.3033592, IEEE Access

processed by the receiver (at the 5G base station or user equipment). During the measurement, we did not place any obstacles on the wireless signal path, though there could be multiple reflections from the walls as described in Fig. 1.

Firstly, we measured the throughput for three different SMF lengths (100, 200, and 300 m) when the wireless-distance was fixed at 2 meters, depicted in Fig. 8. And then, we measured the throughput varying the wireless-distance from 2 to 8 m when the SMF length was fixed to 300 m, illustrated in Fig. 9. The measured throughput did not show a significant change at the various SMF lengths and wireless-distances. For all cases, the DL throughput varied from 700 to 950 Mb/s where its mean value was about 830 Mb/s. Also, the UL throughput was measured to be 100~140 Mb/s over time where its mean value was about 120 Mb/s. The throughput difference between the DL and UL is attributed to the TDD ratio. We attribute the variation of throughput over time not only to the RoF link performance but also to the wireless transmission channels that would have multi-path effects. However, the measurement was mainly limited by the used 5G UE, particularly by the 1GbE adaptor.

Nevertheless, once 4×4 MIMO-operation of the UE becomes available, the throughput will be increased up-to 3.4 Gb/s for DL and 480 Mb/s for UL. The total throughput of the 4×4 MIMO system could be increased potentially up-to ~9 Gb/s as already demonstrated in [17].

IV. FURTHER IMPROVEMENT USING APD

In the proposed system, the total optical loss was 13.5 dB which means that the IFoF link can support 4 optical splitters (50:50 ratio) with 5 RAUs cascaded in series, where each RAU can provide 2×2 MIMO service. In this section, we investigate the feasibility of further increase in the optical power budget beyond 13.5 dB using avalanche photodiode (APD) instead of PIN-PD.

Firstly, we derive the equations to obtain the carrier-to-noise ratio (CNR) of the IFoF system as [20]:

$$CNR_{IFoF} = \left(\frac{1}{CNR_{Thm}} + \frac{1}{CNR_{Shot}} + \frac{1}{CNR_{RIN}} + \frac{1}{CNR_{IMD3}} \right)^{-1} \quad (2)$$

where CNR_{Thm}, CNR_{Shot}, CNR_{RIN}, and CNR_{IMD3} represent the CNR caused by the thermal noise, shot noise, relative intensity noise (RIN) of laser diode, and IMD3 (nonlinear distortion), respectively. The clipping distortion was omitted since its impact is negligible (estimated to be lower than -30 dB) as compared to other terms.

Each term of Eq. 2 can be represented as:

$$CNR_{Thm} = \frac{(mMRP_{rx})^2}{2BNi_{ph}^{\ 2}} \quad (3)$$

$$CNR_{Shot} = \frac{(mMRP_{rx})^2}{4qB(RP_{rx} + i_d)M^2F} \quad (4)$$

$$CNR_{RIN} = \frac{m^2}{2B\gamma_{RIN}} \quad (5)$$

$$CNR_{IMD3} = \frac{P_{IP3}^{\ 2}}{4N_{CTB}P_{rf}^{\ 2}} \quad (6)$$

where the simulation parameters are summarized in the Table-I. The avalanche gain (M) and noise factor (F) can be considered to be 1 for the PIN-PD-based IFoF system. Thus, we obtain the "gain" in terms of the thermal and shot-noise induced CNR by using the APD-based receiver, consequently improving the system performance (i.e., optical power budget). Even though the APD could have worse nonlinear distortion characteristics (i.e. smaller P_{IP3}), the nonlinear distortion is mainly determined by the RF devices such as RF amplifiers and RF mixers etc.

TABLE I
SIMULATION PARAMETERS

Symbol	Quantity	Value
m	optical modulation index per FA	0.035
M	APD's avalanche gain	10
R	PD's responsivity	0.9
P_{rx}	received optical power (dBm)	-25 ~ +5
B	Bandwidth per FA (MHz)	100
N	noise figure of RF amplifier (dB)	7
i_{ph}	Photocurrent	$R \times P_{rx}$
q	electron charge (C)	1.6×10^{-19}
F	APD's noise factor	6.5
γ_{RIN}	relative intensity noise (dB/Hz)	-146
P_{IP3}	3rd order intercept point (mW)	10
N_{CTB}	effective number of third order distortions	9
P_{rf}	input RF power (mW)	0.1

Fig. 10 shows the calculated EVM (= $(1/CNR_{IFoF})^{1/2}$) of FA#5 (i.e., at the middle of the 1.6-2.4 GHz band) of the IFoF transmission link in comparison to the measured values. In the experiment as well as the simulation, we used the set-up depicted in Fig. 3a for two different kinds of PDs (i.e., PIN-PD and APD). The bandwidth of the used APD was about 3.3 GHz, inducing extra penalties to the higher-frequency channels (i.e., 3.6-4.4 GHz). Thus, we perform the comparison at relative low frequency, e.g., 2 GHz to evaluate the relative power budget improvement achieved by the APD. The optical power budget of the IFoF system could be increased by 10 dB with replacing the PIN-PD to the APD. This indicates that we can add 3 of 50:50 optical splitters in series or one 1×8 optical splitter in the optical link. At relatively high received optical power (e.g., >-2 dBm), however, the APD results in slightly worse EVM than that of the PIN-PD. This is because of the avalanche noise factor (F) at the shot-noise that is multiplied to the received optical power.

In this paper, we considered the exploit of 50:50 splitting ratio only, making the EVM performances highly dependent on the RAU numbers as explained in Fig. 6. This could be resolved by using different power splitting ratio such as 90:10 (instead of 50:50) as we calculated in Fig. 11. In the calculation (Fig. 11), we added 0.15 dB excess loss for every single optical splitter. When the PIN-PD is used (where the total optical link loss is allowed to be up-to 13.5 dB), the

This article has been accepted for publication in a future issue of this journal, but has not been fully edited. Content may change prior to final publication. Citation information: DOI 10.1109/ACCESS.2020.3033592, IEEE Access

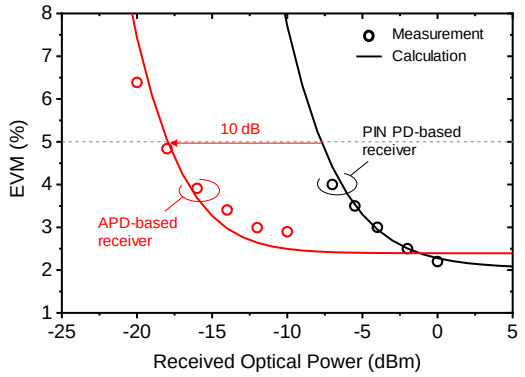

FIGURE 10. Error vector magnitude (EVM) of FA#5 (2.0-2.1 GHz) as a function of the received optical power for two different receivers (APD vs. PIN-PD) (lines: simulation, symbols: measurement).

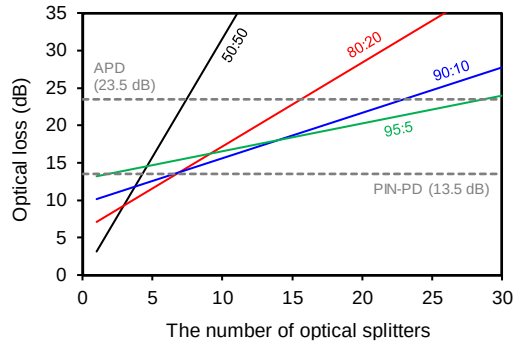

FIGURE 11. Optical loss as a function of the number of optical splitters in the cascaded Radio-over-Fiber (RoF) link for various splitting ratios.

number of cascaded RAUs could be increased up-to 8 by using 90:10 optical splitters, as seen in Fig. 11. Furthermore, in case the APD-based Rx is utilized (where up-to 23.5 dB optical loss is allowed), the number of RAUs could be up-to 29 by using 95:5 optical splitter.

V. CONCLUSION

We proposed and experimentally demonstrated the cascaded DAS for its application in the mmWave-based 5G indoor network. The RoF technology allowed for the efficient configuration of the cascaded architecture, enabling the easy coverage extension as well as the management/installation for the reduced cost and efforts. In particular, we characterized the IFoF transmission link that has the cascade structure by measuring its EVM level to be 5 % or less at the total optical link loss of 13.5 dB. This indicates the use of 4 optical splitters (50:50) that allows for up-to 5 cascaded RAUs in series where its total throughput (considering both the downlink and uplink) was about 1 Gb/s per a single antenna (being ~4 Gb/s in case of the 4×4 MIMO operation), which actually could be improved with an advanced 5G user equipment.

To further increase the optical power budget beyond 13.5 dB, we investigated the use of APD that provided the avalanche gain to the electrical signal, achieving additional optical link budget of 10 dB, corresponding to the optical loss of the 1×8 optical splitter (or three cascaded 1×2 optical splitters). Moreover, the different optical splitting ratio allowed to accommodate more RAUs, e.g., up-to 29 with using APD and 95:5 splitting ratio. We believe the proposed architecture could be also applicable to many different indoor/outdoor systems such as wireless data interconnect and autonomous driving as well as the indoor mobile network.

REFERENCES

[1] 3GPP TR 21.915 v.15.0.0, Summary of Rel-15 Work Items (Release 15), Sep. 2019.
[2] B. Samon, “Setting the scene for 5G: opportunities and challenges,” Int. Telecommun. Union, Switzerland, ITU Report D-PREF-BB.5G, Sep. 2018.
[3] 3GPP TR 38.901 v. 16.1.0, Study on channel model for frequencies from 0.5 to 100 GHz, 2019.
[4] K. Haneda, L. Tian, H. Asplund, J. Li, Y. Wang, D. Steer, C. Li, T. Balercia, S. Lee, Y. Kim, A. Ghosh, T. Thomas, T. Nakamura, Y. Kakishima, T. Imai, H. Papadopoulas, T. S. Rappaport, G. R. MacCartney Jr., M. K. Samimi, S. Sun, O. Koymen, S. Hur, J. Park, J. Zhang, E. Mellios, A. F. Molisch, S. S. Ghassamzadeh, and A. Ghosh, "Indoor 5G 3GPP-like Channel Models for Office and Shopping Mall Environments," presented at the *IEEE ICC2016-Workshops*, Kuala Lumpur, Malaysia, May 23-27, 2016.
[5] J. Du, D. Chizhik, R. Feick, G. Castro, M. Rodriguez, and R. A. Valenzuela, "Suburban Residential Building Penetration Loss at 28 GHz for Fixed Wireless Access," *IEEE Wirel. Commun. Le.*, vol. 7, no. 6, pp.890-893, May 11, 2018, DOI: 10.1109/LWC.2018.2835473 [online].
[6] HetNet Forum, “Distributed antenna system (DAS) and small cell technologies distinguished,” Feb. 2013.
[7] C. Wallace, "Brining 5G networks indoors," Ericsson, Stockholm, Sweden, White Paper EN/LZT 26/28701-FGB 101 0308, Nov. 2019.
[8] CPRI Consortium, “Common public radio interface (CPRI); interface specification,” CPRI specification V7.0, 2015.
[9] “Common public radio interface: eCPRI interface specification,” eCPRI Specification V2.0, May 2019.
[10] J. Kim, M. Sung, E.-S. Kim, S.-H. Cho, and J. H. Lee, “4 × 4 MIMO architecture supporting IFoF-based analog indoor distributed antenna system for 5G mobile communications,” *Opt. Express*, vol. 26, no. 22, pp. 28216–28227, 2018.
[11] S. H. Cho, H. Park, H. S. Chung, K. H. Doo, S. Lee, and J. H. Lee, “Cost-effective next generation mobile fronthaul architecture with multi IF carrier transmission scheme,” in *Proc. Opt. Fiber Commun. Conf. Exhib.*, San Francisco, CA, USA, 2014, Paper Tu2B.6.
[12] J. Bohata, M. Komanec, J. Spacil, Z. Ghassemlooy, S. Zvanovec, and R. Slavik, "24-26 GHz radio-over-fiber and free-space optics for fifth-generation systems," Opt. Lett., vol. 43, no. 5, pp. 1035-1038, 2018.
[13] S. Ishimura, B. G. Kim, K. Tanaka, K. Nishimura, H. Kim, Y. C. Chung, and M. Suzuki, “Broadband IF-Over-Fiber Transmission With Parallel IM/PM Transmitter Overcoming Dispersion-Induced RF Power Fading for High-Capacity Mobile Fronthaul Links,” IEEE Photonics J. vol. 10, no. 1, pp. 7900609, 2018.
[14] H. N. Parajuli, H. Sham, L. G. Gonzalez, E. Udvary, C. Renaud, and J. Mitchell, "Experimental demonstration of multi-Gbps multi sub-bands FBMC transmission in mm-wave radio over a fiber system," Opt. Express, vol. 26, no. 6, pp. 7306-7312, 2018.
[15] C. Browning, E. P. Martin, A. Farhang, and L. P. Barry, "60 GHz 5G Radio-Over-Fiber Using UF-OFDM With Optical Heterodyning," IEEE Photonic. Tech. L., vol. 29, no. 23, pp. 2059-2062, 2017.
[16] J. Kim, M. Sung, S.-H. Cho, Y.-J. Won, B.-C. Lim, S.-Y. Pyun, J.-K. Lee, and J. H. Lee, "MIMO-Supporting Radio-Over-Fiber System and its Application in mmWave-Based Indoor 5G Mobile Network," *J. Lightw. Technol.*, vol. 38, no. 1, pp. 101-111, Jan. 1, 2020.
[17] M. Sung, J. Kim, E.-S. Kim, S.-H. Cho, Y.-J. Won, B.-C. Lim, S.-Y. Pyun, J.-K. Lee, and J. H. Lee, “RoF-Based Radio Access Network for 5G Mobile Communication Systems in 28 GHz Millimeter-

Wave," *J. Lightw. Technol.*, vol. 38, no. 2, pp. 409-420, Jan. 15, 2020.

[18] Z. Yun and M. F. Iskander, "Ray Tracing for Radio Propagation Modeling: Principles and Applications," IEEE Access, vol. 3, pp. 1089-1100, Jul. 8, 2015.

[19] W. Zhu, E. N. Fokoua, Y. Chen, T. Bradley, S. R. Sandoghchi, M. Ding, G. T. Jasion, M. N. Petrovich, F. Poletti, M. Zhao, D. J. Richardson, R. Slavik, "Toward High Accuracy Positioning in 5G via Passive Synchronization of Base Stations Using Thermally-Insensitive Optical Fibers," *IEEE Access*, vol. 7, Aug. 13, 2019.

[20] E.-S. Kim, J. Kim, M. Sung, S.-H. Cho, J. H. Lee, and H. S. Chung, "Power budget improvement of multi-IFoF based analog indoor-distributed antenna system (DAS) with laser over-modulation," *Opt. Commun.*, vol. 435, pp. 129–133, Mar. 2019.

[21] E. E. Bergmann, C. Y. Kuo, and S. Y. Huang, "Dispersion-induced composite second-order distortion at 1.5 um," IEEE Photonic. Tech. L., vol. 3, no. 1, pp. 59?61, Jan. 1991.